

A real-time noise cancelling EEG electrode employing Deep Learning

Henry Cowan¹, Sama Daryanavard¹, Bernd Porr^{1,*}, and Ravinder Dahiya^{2,+}

¹Biomedical Engineering, James Watt School of Engineering, University of Glasgow, Engineering, University of Glasgow, G12 8QQ, UK

²Bendable Electronics and Sensing Technologies (BEST) group, James Watt School of Engineering, University of Glasgow, G12 8QQ, UK

*bernd.porr@glasgow.ac.uk

+Ravinder.Dahiya@glasgow.ac.uk

ABSTRACT

Two major problems of head worn electroencephalogram (EEG) are muscle and eye-blink artefacts, in particular in non-clinical environments while performing everyday tasks. Current artefact removal techniques such as principle component analysis (PCA) or independent component analysis (ICA) take signals from a high number of electrodes and separate the noise from the signal by processing them offline in a computationally expensive and slow way. In contrast, we present a smart compound electrode which is able to learn in real-time to remove artefacts. The smart 3D printed electrode consists of a central electrode and a ring electrode where poly-lactate acid (PLA) was used for the the base and Ag/AgCl for the conductive parts allowing standard manufacturing processes. A new deep learning algorithm then learns continuously to remove both eye-blink and muscle artefacts which combines the real-time capabilities of adaptive filters with the power of deep neural networks. The electrode setup together with the deep learning algorithm increases the signal to noise ratio of the EEG in average by 20 dB. Our approach offers a simple 3D printed design in combination with a real-time algorithm which can be integrated into the electrode itself. This electrode has the potential to provide high quality EEG in non-clinical and consumer applications, such as sleep monitoring and brain-computer interface (BCI).

Introduction

The detection of electrical activity in the brain, the electroencephalogram (EEG), has many popular applications ranging from epilepsy detection to brain computer interfaces¹⁻³. However, EEG being a small signal, is contaminated with noise from numerous sources, often orders of magnitude larger than the signal⁴. On the one hand EEG is contaminated by measurement noise originating from the electrode cables, mains noise and variable electrode impedance which can be minimised by improving the measurement hardware itself. On the other hand physiological artefacts are harder to control or remove such as electrooculogram (EOG), blinking, and in particular facial electromyogram (EMG) activity as its frequency spectrum overlaps with that of the EEG signals⁵.

In order to increase the signal to noise ratio (SNR) of the EEG signal one can divide the approaches into two categories: electrode design and post-processing. With respect to the latter: by far the most popular approach is principle component analysis (PCA) or independent component analysis (ICA) where the algorithms separate the EEG signals from noise^{4,6-9} by assuming that channels contains both noise and signal in different amplitudes and spatial distribution so that algorithms such as ICA or PCA can separate them. However, both PCA and ICA are not real-time algorithms because they first analyse the signals and then separate them. This analysis is offline, requires the signal and noise relationships to be constant over time, and demands high computational power.

Most popular alternatives to the computationally intensive PCA/ICA are real-time algorithms which use the wavelet transform which are by far inferior in their performance^{10,11}. For real-time applications one needs to resort to direct causal filtering techniques using bandpass filters, the short time Fourier Transform or wavelet transform in the frequency domain¹² or applying a chain of derivatives in the time-domain¹³ – which effectively are highpass filters at increasing order and might just amplify EMG noise. A promising approach is adaptive filtering. The noise is removed by an adaptive algorithm which uses information about the noise from additional electrodes^{14,15}. Such algorithms can run in real-time but need these additional electrodes similar to the capacitive EEG⁹ to provide information about the noise. Again, this calls for the design and manufacture of dedicated electrodes which record signal and noise separately to then compute a noise-free signal. This leads us to the mechanical design of EEG electrodes to reduce noise.

The mechanical EEG electrodes design is as old as the first EEG recordings¹⁶ and the standard Ag/AgCl cup electrodes

have been the main staple of EEG recordings ever since¹⁷. A major concern has always been the electrode resistance with the skin¹⁸ which has an impact on the signal to noise ratio of the EEG. The electrode resistance has become even more of a concern with the advent of BCI and consumer EEG headbands which favour dry electrodes¹⁹. Besides active electrodes²⁰ novel electrode designs promise to help reduce the electrode resistance^{21,22} in particular by using spring contact probes^{23,24}. However, these electrode designs only improve the signal to noise ratio by a better skin/electrode contact but do not take into account the spatial distribution of signals versus noise which calls for compound electrodes.

As mentioned earlier, there is a general consensus that noise originates from further afield and is present globally. In contrast the EEG signal is assumed to originate locally. For example the jaw or facial muscles are further away than the localised EEG underneath an electrode. The next step is thus to recruit numerous electrodes and combine them electrically or mathematically into a compound electrode²⁵ which exploits the fact that EEG emerges locally underneath the electrode but noise emerges globally or further afield. The most popular compound electrode or “montage” which utilises this is the spatial Laplace operator²⁶, where effectively the local spatial difference between a centre electrode and a ring electrode or multiple ring electrodes is calculated²⁷. This montage ensures that if a signal is common to the detection electrode and the surrounding reference electrodes (i.e. low spatial resolution), the signal will be attenuated on the detection electrode. However, if the signal underneath the detection electrode is not common to the surrounding electrodes, it will not be removed. As EEG is more spatially localised than EMG/EOG or blinking artefacts it can be said that these artefacts will be attenuated whilst the EEG is retained, resulting in an increased signal-to-noise ratio (SNR)^{26–30}. The advantage of the Laplace montage is that it is highly focal and avoids reference contamination as only the nearest surrounding electrodes are considered. A Laplace electrode however, has the shortcoming that its computations are fixed so that changing electrode properties and changing correlations between the rings cannot be corrected. While Laplace electrodes are perfect in theory, in practice the relationship between the EEG generated in the brain and the resulting signal at the electrode is complex and changes over time. This holds even more so for the noise as the relationship between noise and signal changes over time. This calls for a smart compound electrode which implements an adaptive Laplacian operator which continuously learns about the changing signal and noise conditions. In this paper we present a novel compound electrode which can be easily 3D printed and employs a new deep learning algorithm to adaptively remove the noise from the EEG. We show this by first removing eye-blink artefacts and then muscle noise.

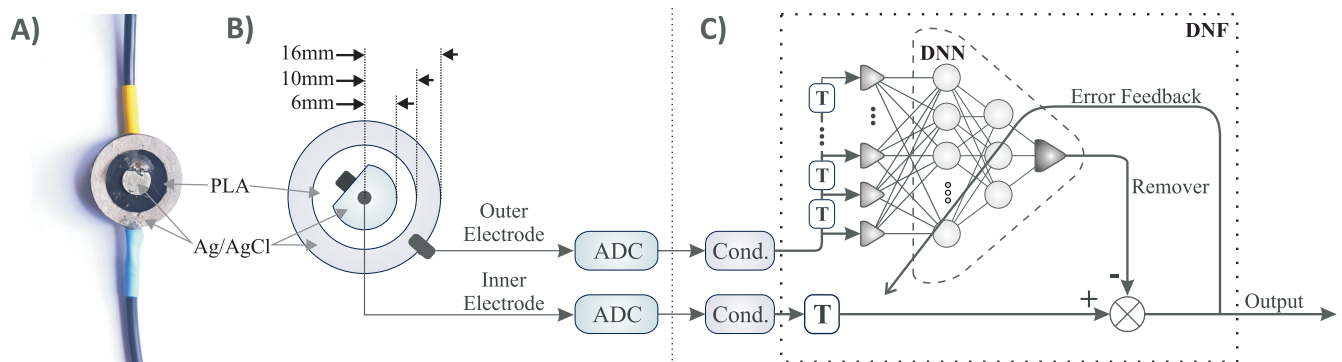


Figure 1. A) Photo of the manufactured compound electrode. The top wire connects to the inner electrode. The bottom wire to the outer electrode. B) Top view of the new compound electrode with the inner electrode and the outer electrode. The substrate of the electrode was PLA and the inner and outer electrodes were Ag/AgCl painted on the PLA. C) Signal processing of the two signals originating from the inner and outer ring electrodes: ADC = Analogue Digital Converter, Cond. = standard signal conditioning such as DC/50Hz removal. T = time delay.

Results

Working principle of the smart electrode. As outlined in the introduction, we assume that the EEG originates *locally* from a small surface area of the head and that artefacts originate further afield and, therefore, they have a *global* and uniform strength across the head of the subject. Consequently, a compound electrode consisting of a small inner electrode and a larger ring electrode will then pick up the *EEG* mostly from the *inner* electrode. However, the *noise* will be present on *both the inner and outer* electrodes (Fig. 1A,B) which can be summarised as:

$$\text{inner electrode} = \text{EEG} + \text{noise} \quad (1)$$

$$\text{outer electrode} = \text{noise} \quad (2)$$

The goal of the learning algorithm is to render the signal from the inner electrode as noise free as possible. Theoretically, one could simply subtract the outer electrode signal (Eq. 2) from the inner one (Eq. 1) to obtain a noise free EEG but in practice this is not possible because of changing electrode and noise characteristics. Instead, a machine learning algorithm learns, in real-time, how to alter the signal from the outer electrode in a way that it perfectly eliminates the noise from the inner electrode which then results in a noise-free EEG signal. In the next two sections we describe first, the electrode and then the algorithm.

Fabrication of the compound electrode. The physical design of the electrode was driven by durability, ease of manufacture and reliability. Our new smart electrode consists of two raised ring portions separated by a channel, the outer ring with a larger surface area than the inner. Given the relative complexity of the concentric ring design, the fact that 3D printing of electrodes has recently become popular^{22,31,32} and the recent successes the group has had with 3D-printed sensors³³, 3D printing was chosen for the electrodes manufacture. Having determined the flexibility and 3D-printability requirements along with the hegemonic requirement of biocompatibility, the final fundamental requirement is that of adhesion of the conductive layer to the backing material. This property is crucial for a robust electrode design as flaking of the conductive layer can reduce the electrode's conductivity³⁴. Using this extensive criterion, it was determined that Polylactate acid (PLA) was the most suitable material. Not only is PLA cheap, flexible, 3D-printable, chemically stable and readily available, the adhesion qualities of Ag/AgCl to the PLA had previously been determined suitable in similar applications³¹. After 3D printing of the PLA base a thin layer of Ag/AgCl paste was deposited on each of the raised rings using a plastic spatula. The Ag/AgCl was then cured at 70°C for 1 hour. Figure 1 A shows the final printed electrode with Ag/AgCl applied. When compared with current gold/platinum electrodes which are rigid and can be uncomfortable^{35,36}, the use of an Ag/AgCl paste on a flexible substrate is advantageous as it allows a degree of flexibility to the electrode ensuring an optimal skin-electrode contact area, in turn decreasing the inter-electrode impedance resulting in an increased SNR for that electrode whilst also increasing the comfort for the patient³⁷. This makes the novel, compound electrode significantly more useful and suitable for long-term monitoring applications. Wires were connected to the electrode substrate by melting the wires into the flexible PLA structure using a soldering iron, then applying pure silver paste to ensure electrical contact, and epoxy to solidify the connection. This electrode has proven to be robust and easy to both manufacture and integrate into a headband or EEG cap as a wearable device.

Recording of the two signals from the compound electrode Two signals were recorded with a DC coupled bio-amplifier (Attys, Glasgow Neuro LTD) from the inner and outer portions of the smart electrode (Fig. 1B) which was placed on the forehead (Fp1) and mechanically kept in place with a standard headband. The reference Ag/AgCl electrode was placed on the cheek of the subject and this was done solely for practical reasons: to have only the smart electrode under the headband and thus being able to focus on its performance. The data was digitised (ADC) as it was measured at the electrodes without any analogue filtering³⁸.

Using a deep neural network to minimise the noise Fig. 1C shows the block diagram of our novel deep neuronal network (DNN) which in conjunction with the additional building blocks becomes a deep neuronal *filter* (DNF) to remove noise³⁸. Before being fed into the DNF the data from both channels undergo standard DC and mains noise removal ("Cond."). No other pre-processing was performed. This means that the differences between the inner and outer electrode signals are purely based on the mechanical and electrical design of the electrode as described in the previous section.

Recall that the deep network exploits the assumption that the outer electrode contains just the noise (Eq. 2) and that the network learns to subtract this from the signal from the inner electrode (Eq. 2) at the summation node "X". The teaching signal of the network is the actual output signal of the network as in any other standard noise cancellation framework. This means that the network will remove any noise from the outer electrode which is correlated with noise from the inner electrode. However, because the outer and inner electrodes having different shapes the noise will be different between the inner and outer electrodes. In order to give the DNN any opportunity to learn a perfect "Remover" (see Fig. 1C) it needs to act as a digital filter. Inspired by a Finite Impulse Response (FIR) filter, we send the signal through a delay line and then feed it into our DNN. This then gives the DNN the flexibility to learn different filter characteristics and to generate an output signal which is then subtracted from the incoming signal from the inner electrode, which is also delayed, resulting in the final output signal. This output is the filtered EEG which is also the error signal for the DNN and is back-propagated for real-time learning. More specifically, the common components in the output signal and the outer electrode signal correlate to change the weights of the neural network and thus trying to minimise the noise present at the inner electrode. The learning is real-time and "on" (i.e. in effect) at all times, meaning, the network adjusts to the changes in the electrode contact as they happen. The learning rate of the DNN determines how fast the electrode adapts.

Noise reduction for eye-blinks and alpha waves. In order to evaluate the performance of our smart electrode we conducted two separate experiments where the network attempts to remove different artefacts. In the first experiment we investigated the reduction of eye-blink artefacts while having the eyes open and in the 2nd experiment we looked at the reduction of EMG

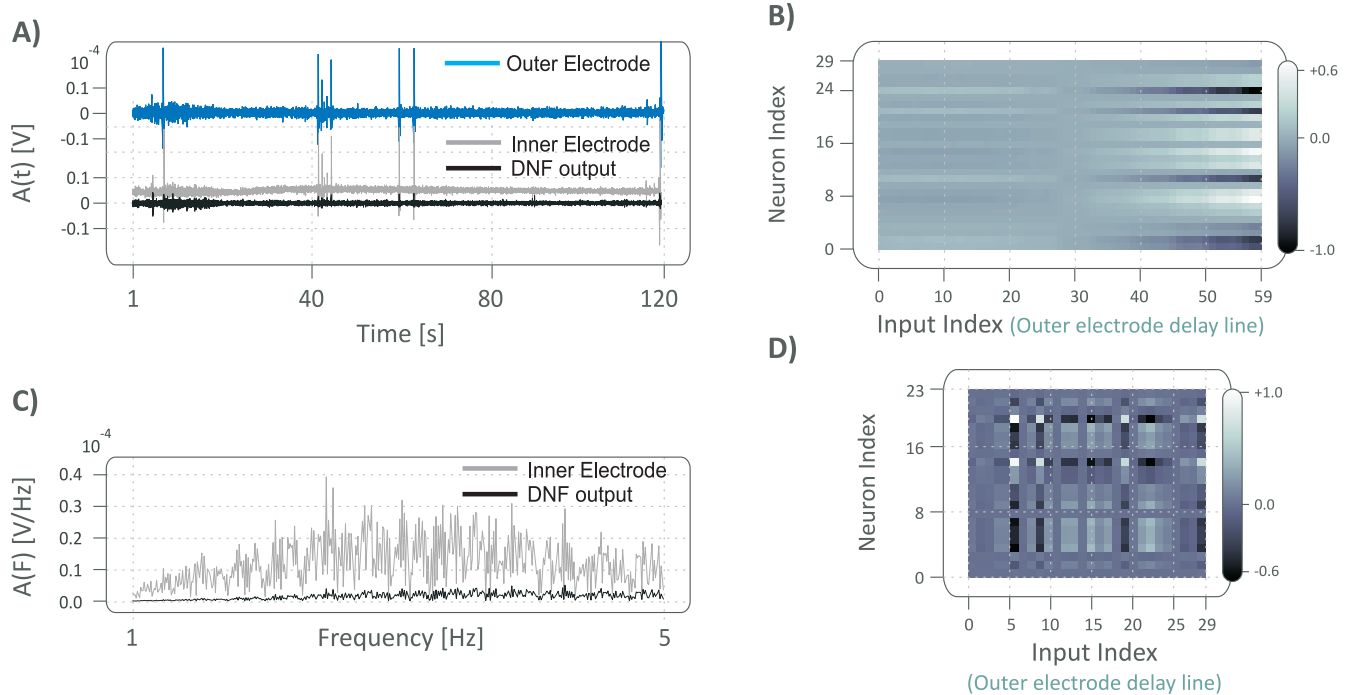


Figure 2. Eyeblick removal **A)** Time domain signals $A(t)$ from the outer part of the smart electrode (blue), the inner part (grey) and the output of the DNF (black) in volt against seconds. **B)** Weight matrix from the input layer to the 1st hidden layer of the DNN. x-axis: neuron index number of the input neuron which connect to the delay line of the outer electrode signal (see Fig. 1) so that “input index” = 0 has the un-delayed signal, index one the signal delayed by one time steps and so forth. y-axis is the index of the target neuron in the 1st hidden layer. **C)** Frequency spectrum $A(F)$ of the inner electrode and the output of the DNF. **D)** Weight matrix from the 1st hidden layer to the 2nd hidden layer of the DNF where the x-axis is the neuron index of the 1st layer and matches the y-axis in B). The y-axis here represents the index number of the target neuron in the next deeper layer.

artefacts with eyes closed:

1. Delta frequency region: removal of eye-blink artefacts (eyes open)
2. Alpha frequency region: removal of muscle noise (eyes closed)

We are now going to present the results of these two different experiments.

Reduction of eye-blink artefacts. Fig. 2 shows an example of data collected while the subject is having the eyes open. The main artefact here are eye-blinks which can be seen in Fig. 2A, which appear as large spikes in both the inner and outer electrode and having approximately the temporal duration of the actual mechanical eye-blink. Because of their pulse like shape they generate a wide low frequency spectrum (Fig. 2B) and render the delta band, in particular, unusable. Thus, eye-blinks are unwanted and need to be removed for the recording.

As outlined above, the central idea is that the artefact is present at both the inner and outer electrode and the DNF exploits this to remove the artefact. Indeed, Fig. 2A shows that the eye blink artefact is present in both the inner and outer electrode. The eye-blink is spatially distributed over a large part of the head and consequently affects both the inner and outer electrode. The DNF learns now to remove the eye-blink from the inner electrode’s signal (grey) by using the eye-blinks from the outer electrodes as the teaching signal which is shown as a blue trace in Fig. 2A. In the time-domain this leads to the removal of the spike-like eye blinks in Fig. 2A and to a dramatic reduction of the wideband noise in the delta band in Fig. 2C, in black trace.

To gain an insight into what the network has learned, we have plotted the weight matrix of the first layer and that of the second layer in Fig. 2B,D respectively. Fig. 2B shows the weights from the input delay line (see Fig. 1C) to the 1st hidden layer. Most neurons learn sinewave-like low frequency detectors with different phases so that the 1st layer acts like a low frequency filter for the deeper layers. As expected the deeper layers develop complex receptive fields which are not easy to interpret but show that the DNN uses its individual neurons for different purposes and not just trivial operations.

As a next step we investigate the higher frequency regions which are contaminated by muscle noise.

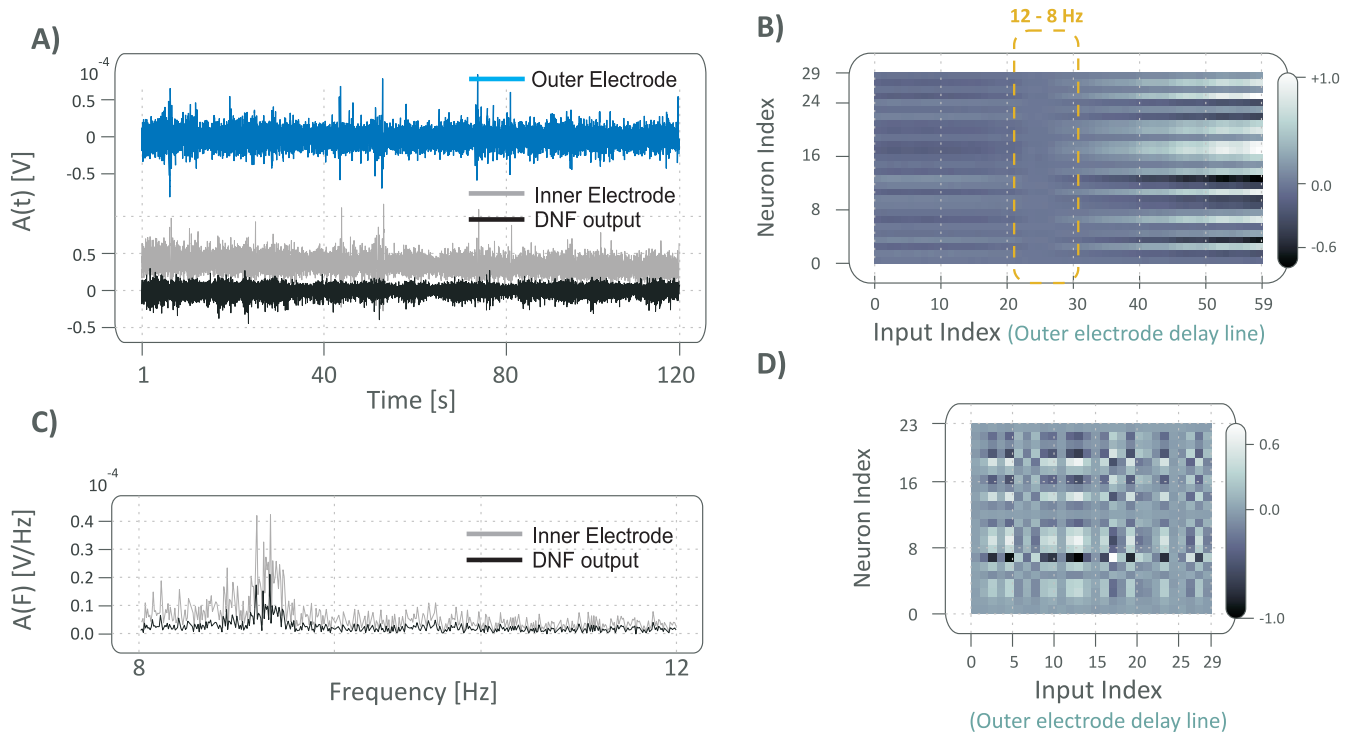


Figure 3. Facial muscle EMG removal **A)** Time-domain signals $A(t)$ from the outer part of the smart electrode (blue), the inner part (grey) and the output of the DNF (black) in volt against seconds. **B)** Weight matrix from the input layer to the 1st hidden layer of the DNN. x-axis: neuron index number of the input neuron which connect to the delay line of the outer electrode signal (see Fig. 1) so that “input index” = 0 has the un-delayed signal, then index one is the signal delayed by one time steps and so forth. The y-axis is the index of the target neuron in the 1st hidden layer. **C)** Frequency spectrum $A(F)$ of the inner electrode and the output of the DNF. **D)** Weight matrix from the 1st hidden layer to the 2nd hidden layer of the DNF where the x-axis is the neuron index of the 1st layer and matches the y-axis in B). The y-axis here represents the index number of the target neuron in the next deeper layer.

Reduction of muscle artefacts. Muscle artefacts are wideband noise polluting higher EEG frequency bands such as the alpha or gamma band. We focus here on the alpha band because, when the eyes are closed, has a peak at approximately 10 Hz, the alpha peak. This also has the advantage that we have no eye blink artefacts so that the DNF can just focus on the EMG activity exclusively.

Muscle activity (EMG) is random noise which is superimposed on the EEG. Fig. 3A shows the time-domain signals from the inner and outer parts of our smart electrode (grey and blue, respectively). The EMG originates mainly from facial muscles like the jaw muscle or the eyebrow muscles and is again present in both the inner and the outer electrodes. Fig. 3C shows the frequency spectrum of the inner electrode (grey) and an alpha peak at 10 Hz is visible. Note that there is a large variability between subjects where the alpha peak is more pronounced with some and less with others. Since the eyes are closed no eye blinks are present and the main noise originates from facial muscles which is picked up by both the inner and outer electrodes.

The black traces in Fig. 3A,C represent the output of the DNF. In the time-domain plot Fig. 3A the amplitude of the signal is reduced, however, to gain a better understanding of the filtering we need to switch to the frequency domain (Fig. 3C) where the noise outwith the alpha band has been reduced, both below and above the alpha peak at 10 Hz. Fig. 3B,D shows the matrix of weights in the input layer. For the input layer of the DNN Fig. 3B shows that there is a noticeable band around input index 25 which corresponds to a delay of 10 ms which in turn is the period of the Alpha frequency (given a sampling rate of 250 Hz). A simple interpretation is that the alpha period of 10 ms is not boosted by the weight choices but twice the period at 20 ms (Input index 50) is. However, weights at index 50 have both negative and positive values and the corresponding signals are then processed differently in the deeper layer Fig. 3D. This points to a specific learning about the 10 Hz alpha peak and not to remove it. However, we should note that the alpha peak is reduced in amplitude which is expected as there is a weak correlation of the alpha activity between the inner and outer electrode which results in a partial removal of the alpha activity. This is due to alpha mainly originating from occipital regions of the brain but we measure at the front which will be partially

interpreted as a global signal and thus be removed. However, the crucial observation is how much the signal to noise ratio has been improved which will be evaluated next for both the eye-blink case and the alpha waves.

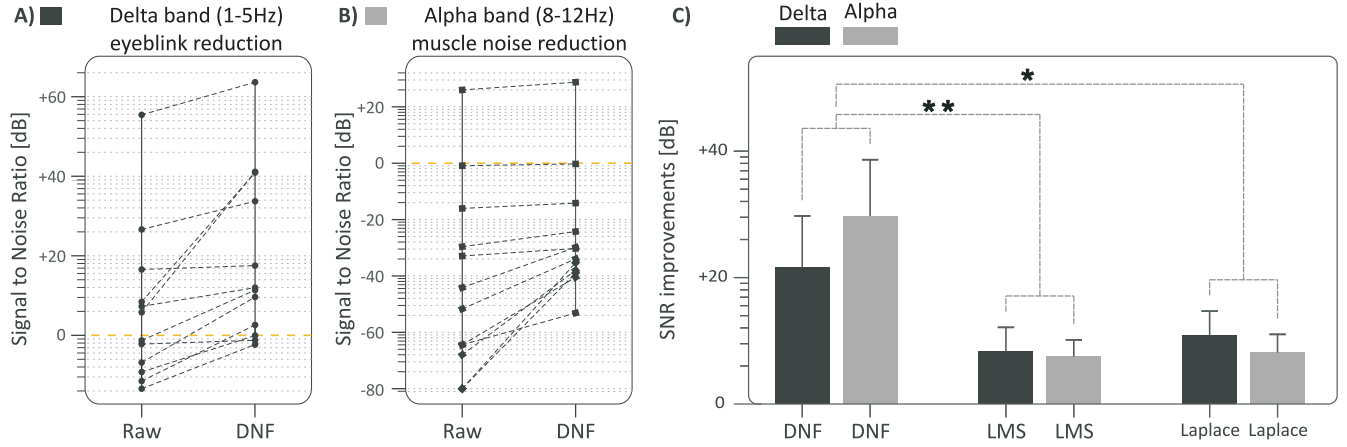


Figure 4. *A,B*) Improvement of the signal to noise ratios. Plotted are the signal to noise ratios in dB of the Raw signal traces (just with DC and 50 Hz removed) and the filtered signals by our smart electrode (DNF). Every of the 12 subjects is indicated by a black dot. The dashed lines between the “Raw” plot and the “DNF” plot indicate which dots belong to the same subject so that it is possible to track the individual improvements. *A*) The delta frequency experiment which learns to remove eye-blinks and improves the signal to noise ratio between delta waves and eye-blinks. *B*) The alpha frequency experiment which learns to remove muscle activity and improves the signal to noise ratio between alpha waves and muscle activity. *C*) Comparison of the signal to noise improvements between our DNF, LMS algorithm and a hard wired Laplacian operator. The two boxes for DNF directly correspond to the results in *A,B*) for the separate delta and alpha band improvements.

Approximating the signal to noise ratios. In order to calculate the *signal to noise ratio* we need to have access to the *signal* and *noise* exclusively.¹ In the case of the eye-blinks the *noise* originates from the eye muscles, whereas, the *signal* is the underlying EEG. However, even data that does not contain eye-blinks noise, does contain muscle activity. To remove the muscle activity, one needs to paralyse the subject and this is, of course, not feasible. In order to overcome this we can use as a *signal* the data from the alpha waves experiment because the eyes were closed and consequently is free of eye blinks. This is of course just a relative measure for the reduction of the eye-blink artefacts. This can then be evaluated for both the raw signals (with just DC and mains removed) and the signals at the output of our DNF. For the eye-blink we can thus evaluate the relative signal to noise ratio by integrating over the frequency spectra $A(F)$ as shown in Fig. 2C & Fig. 2C as:

$$SNR^{\text{delta}} = \frac{\int_{1\text{Hz}}^{5\text{Hz}} A(F)_{\text{eyes closed}}}{\int_{1\text{Hz}}^{5\text{Hz}} A(F)_{\text{eyes open}} - \int_{1\text{Hz}}^{5\text{Hz}} A(F)_{\text{eyes closed}}} \quad (3)$$

where the amplitude of the *signal* is derived from the eyes closed condition by integrating over the 1 – 5 Hz band of the frequency spectrum of the *signal* and the *noise* from the eyes open condition minus the integral of the eyes closed condition. Fig. 4A shows the SNR of all 12 subjects for the delta band in dB before and after filtering by our DNN. It can be seen that all SNRs have significantly ($p < 0.05$) improved after being filtered by our DNN.

Similarly, for the alpha frequencies we can calculate relative signal to noise ratios where we assume that EEG alpha waves only appear while the eyes are closed and that we assume that in the eyes open condition we have only noise:

$$SNR^{\text{alpha}} = \frac{\int_{8\text{Hz}}^{12\text{Hz}} A(F)_{\text{eyes closed}} - \int_{8\text{Hz}}^{12\text{Hz}} A(F)_{\text{eyes open}}}{\int_{8\text{Hz}}^{12\text{Hz}} A(F)_{\text{eyes open}}} \quad (4)$$

where Fig. 4B shows the results for the SNR again for the raw signals and the filtered ones by our DNN. Again, the SNR is significantly ($p < 0.05$) improved in all subjects. Note that these results are only a rough estimate because of low subject numbers but also given the relative SNRs. For that reason we have shown the individual subjects and their improvements by our electrode where the different cases can differ substantially. This has of course many reasons given the variability of the

¹If referred to signal and noise in terms of the *signal to noise ratio* the words *signal* and *noise* are in italic.

data from different subjects and also different levels of noise depending on electrode contact, the subject's ability to relax and interpersonal differences of EEG activity. Finally, we have compared the performance of our new DNF electrode with a standard Least Mean Square (LMS) filter and that of a Laplace operator in Fig. 4C. The two bars for SNR improvement with a DNF directly correspond to Fig. 4A,B and show that there is on average more than 20 dB improvement of the SNR, of course with a large standard deviation because of inter-subject differences. The results for LMS are significantly worse than for the DNF for both delta and alpha waves. This shows the power of a deep network with non-linear activation functions against a shallow single layer linear network as it is the case for the LMS filter. Finally we created a Laplace operator where we simply subtracted the signal from the outer ring electrode from that of the inner electrode. This yielded similar SNR improvements as for the LMS filter and is not surprising as the LMS filter being a linear operator should learn to subtract the outer signal from the inner and indeed it does. The Laplace filter approach leads to improvements of about 5 dB and this is just due to the electrode configuration itself. However the significantly more powerful approach is to combine the compound electrode with a deep network filter (DNF).

Discussion

The spatial distribution of the electrodes is crucial to reducing noise in EEG and has been in particular investigated with the rise of brain computer interfaces (BCI) where often the user is actively using their muscles and thus creating a large amount of both EMG and movement artefacts³⁹. It could be shown that the central average reference (CAR) and both small and large Laplacian montages²⁶ are effective in improving the signal to noise ratios. This has been shown for ECG²⁹ by removing movement artefacts and for EEG³⁰. Common to all approaches is the approximation and optimisation of a 2D spatial Laplace operator^{26,27,40}. The more rings are employed at an optimal spacing the more efficient the operator will be. The calculation of the Laplacian is usually performed by the electrical summation of the EEG sources under each ring, digitised and then subtracted from each other. However, this assumes that every ring can perform a perfect analogue spatial averaging operation which is not the case in practice as electrode impedances will be inhomogeneous and changing over time. The analogue averaging over a ring can be overcome by measuring from a large number of electrodes from an EEG cap and then approximating the Laplace purely in software²⁸ - but this is computationally expensive and if using a standard EEG cap, has its limitations in spatial resolution. On the other hand, the above discussed concentric ring electrode is certainly the most feasible and practical hardware design²⁶, however, has the drawback of assuming perfect recording conditions only present in ideal biophysical models but not in real setups. To overcome its shortcomings of hard wired computations based on ideal models we use an adaptive algorithm to account for the imperfect nature of the electrodes and the dynamic changes of electrode resistance over time, in particular when using dry electrodes.

A particular area of concern is the choice of the adequate conductive electrode material. Bio-electrodes are in contact with the body and will in turn, be exposed to biological electrolytes which can, over time, cause oxidation of the electrode and degrade the electrode's quality^{36,41,42}. It can be concluded that precious metals are the obvious choice for conductive material and many EEG electrodes utilise them to provide the electrode conductivity^{35,43}. Due to the cost of such metals, a superficial, thin coating is usually applied to a cheaper backing material^{22,44}, to provide high conductivity, good chemical stability and structural support for the electrode, simultaneously minimising the cost⁴⁵. The conductive layer selected for the design discussed in this paper was also Ag/AgCl and was selected due to its high conductivity (low resistivity)²², chemical and electrical stability³⁶ and relative manufacturing simplicity (can be printed as an ink^{22,46}).

The least mean squares (LMS) technique to reduce noise in signals is well established, where an FIR filter is trained to reduce the noise in a signal⁴⁷ with the help of one or more reference signals⁴. This has been shown to be effective against EOG by using as a reference both the horizontal and vertical EOG to remove the artefacts from an EEG¹⁵ but requires additional conventional electrodes placed above/below and left/right of the eyes. There have been various approaches of using neural networks to generate the signal (called here "remover") which is used to eliminate the artefacts in the EEG signal⁴⁸.

Previous approaches of creating a network also realised that non-linear filtering of the input variables is essential to achieving reasonable elimination of artefacts. While we used a deep net with non-linear activation functions⁴⁹ others used radial basis functions⁵⁰ or functional link neural networks (FLNN) to generate nonlinear decision boundaries with non-linear functional expansion⁵¹. Even more computationally expensive is an approach where the shortcomings of the FLNN are reduced with the help of an adaptive neural fuzzy inference system⁵². In contrast our deep network operates as a standard deep net and off-the-shelf optimised architectures are readily available. Note that the adaptive filtering approaches above assume that a clean reference signal is available such as EOG or EMG. Instead, we only assume that there is a strong correlation between the signals from the inner and outer electrodes of our smart electrode which means that the noise is coded in the correlation between these two signals, as opposed to a clean and exclusive noise reference.

Instead of employing an adaptive filter which receives as a reference of the noise one can also take a contrary approach and train a neural network with a clean EEG signal as a reference where after training the network then directly outputs the clean signal^{53,54}. This assumes that the clean signal is available which is impossible for muscle noise as the subject cannot be

paralysed and for eye-blinks only between eye-blinks or with eyes closed. In order to overcome this problem one needs to add eye-blinks artificially to clean EEG data and then train the network to remove it⁵⁴. In addition this approach calls for creating chunks of data which are fed into the neural network which then cause problems when the eye-blink spans two chunks⁵³. Given that a noise free EEG is not available the above neural network approaches rather rely on separate measurements of signal and noise which ranges from impractical to impossible. However, in our approach we use the readily available noise as a reference which can be measured with our compound electrode in real-time.

Methods

Compound electrode. A structure was created on SolidWorks 3D modelling software consisting of two raised ring portions separated by a channel, the outer ring with a larger surface area than the inner. This structure was 3D-printed using a polylactide (PLA) polymer. A thin layer of Ag/AgCl paste was deposited on each of the raised rings using a plastic spatula. The Ag/AgCl was cured at 70°C for 1 hour. Wires were connected by melting the wires into the PLA structure using a soldering iron then applying silver paste to ensure electrical contact, and epoxy similar to the other designs. Similar resistances were measured from wire end to conductive plate (1Ω) and the design appeared sturdy.

The areas of the different electrode compounds were:

$$\begin{aligned}
 A_{InnerRing} &= \pi \times 6mm^2 = 113mm^2 \\
 A_{OuterRing} &= A_{Outside} - A_{Inside} \\
 A_{Outside} &= \pi \times 15mm^2 = 707mm^2 \\
 A_{Inside} &= \pi \times 10mm^2 = 314mm^2 \\
 A_{OuterRing} &= 530mm - 78mm \approx 393mm^2
 \end{aligned} \tag{5}$$

An increase of area of the outer ring to the inner ring will effect the impedance characteristics of the electrode, however as the Ag/AgCl electrodes are predominantly resistive components, it will have a minimal effect on the overall impedance of this ring.

Experimental setup for EEG recording. Our compound electrode was situated in an elastic headband with the wires secured within to reduce electromagnetic noise from wire motion. The headband and compound electrode were placed on the subject's head with the Attys biosignal amplifier attached to the rear of the headband. The ground and reference electrodes were commercial Dormo[®] Ag/AgCl wet electrodes and were situated on the subjects left and right cheek. These were placed as close as possible to the headband but not underneath so that the headband solely provided pressure for the compound electrode but at the same time simulating an EEG headband as close as possible.

Ethical approval for this experiment was obtained from the Glasgow University's research ethics committee.

The subject was seated on a chair in a quiet room and was asked to relax. Once the subject had rested a small smear of 10/20[®] conductive gel was applied to the region of the head which would be in electrode contact. The compound electrode was situated in a headband which was then placed over the subject's head, ensuring the electrode made good contact with the forehead. The Attys amplifier was attached to the rear of the headband and connected to the electrode. Channel one was connected to the inner ring of the electrode and channel two was connected to the outer ring. The negative input (reference) and ground connection of the amplifier were connected to each cheek. Note that the reference and the ground electrodes were placed on the cheeks as to simulate an EEG headband by minimising their distance to the electrode; placing them underneath the headband would impose difficulties in adjusting the electrode.

Two sets of data were recorded (eyes open, eyes closed), with the same instructions. A total of 12 subjects were tested. Eleven of the Twelve subjects were aged between 18 and 25 years with the last participant aged 57 years old. All of the subjects were healthy individuals.

Deep learner The data were pre-processed in C++ using an FIR filter which was designed with a high-pass response at 1Hz to remove any DC offset and baseline drift from the trial data, and a band-stop response at 45 – 55 Hz to remove any residual mains noise from the signal. The filter response was generated with 250 taps (1Hz resolution) for both inner and outer electrode channels. The number of taps are kept to a minimum to decrease the delay of the system. As explained above the signal from the outer electrode undergoes further delay caused by the delay line of 59 time steps, and the inner electrode is accordingly delayed by 59 samples to synchronise the filtering at "X" point in Fig.1C.

The network used for DNF is a feed forward neural network with fully connected layers designed with 10 hidden layers, consisting of 29, 23, 19, 17, 13, 11, 7, 5, 3 and 2 neurons in each hidden layer respectively as well as 1 neuron in the output layer. Furthermore, there were 59 inputs to the network obtained form the taps of delay line for outer electrode signal as shown in Fig.1. The weights and biases of the neurons were initialised to a random value in the range of (0, 1], generated by

random seed of 1 (using `std::srand(1)`). Eq.6 below shows the forward propagation of the outer electrode signal S^{outer} through the first hidden layer of the network:

$$A_j^1 = \sigma(Z_j^1) = \sigma(\sum_{k=1}^{59} (\omega_{kj}^1 S_k^{outer}) + b_j^1) \quad (6)$$

Where S_k^{outer} is the signal from the k^{th} tap of the delay line for the outer electrode signal (Fig.1) with k varying from 1 to 59. Using the internal parameters of the neurons in this layer, weights ω_{kj}^1 and biases b_j^1 , this weighted sum results in the sum of this neuron Z_j^1 and sigmoid function acting on this sum results in the activation of this neuron A_j^1 . Similarly, these activations propagate through the deeper layers in the network as follow:

$$A_j^\ell = \sigma(Z_j^\ell) = \sigma(\sum_{i=1}^I (\omega_{ij}^\ell A_i^{\ell-1}) + b_j^\ell) \quad \text{where: } \ell : 2, \dots, 10 \quad (7)$$

Finally, in the output layer this weighted sum results in the generation of the ‘‘Remover’’ signal as follows:

$$S^{remover} = \sigma(Z_1^{11}) = \sigma(\sum_{i=1}^2 (\omega_{i1}^{11} A_i^{10}) + b_1^{11}) \quad (8)$$

Where $S^{remover}$ is the remover signal that is subtracted from the incoming signal from the inner electrode S^{Inner} which is also delayed by 59 time steps for synchronisation; this results in the final output of the DNF as follows:

$$S^{Output} = S^{Inner} - S^{Remover} \quad (9)$$

As explained in the previous sections, the output of the DNF is the noise-free EEG signal and is used for the learning of the neural network using the commonly used gradient decent method called back-propagation. The so called internal error δ_j^ℓ of neurons is defined as below for the output layer:

$$\delta^{11} = S^{output} * \sigma'(Z^{11}) \quad (10)$$

And for deeper layers this is defined through the back-propagation as:

$$\delta_j^\ell = \sum_{k=1}^K (w_{jk}^{\ell+1} \delta_k^{\ell+1}) * \sigma'(Z_j^\ell) \quad \text{where: } \ell : 10, \dots, 1 \quad (11)$$

The changes in weights and biases that cause the optimum reduction in noise is dictated by gradient descent rule as follow:

$$\Delta \omega_{ij}^\ell = \eta_1 \delta_j^\ell * A_i^{\ell-1} \quad \text{and} \quad \Delta b_j^\ell = \eta_2 \delta_j^\ell \quad (12)$$

Where η_1 set to 1 and η_2 set to 2 are the learning rates for weights and biases respectively. Note that the internal error and the activation of each neuron carry information about the frequency build-up of the output signal and the outer electrode signal, respectively. So long as these two signals retain a high correlation ($\delta_j^\ell * A_i^{\ell-1} \equiv S^{Output} * S^{Outer}$ is significant), the weights of the network change to reduce this correlation. The learning converges when the correlation of these two signals is negligible, meaning no frequency components of the noise present in the outer electrode signal is remained in the output of the DNF filter and thus the noise is filtered.

Statistical significance was tested using a paired T-test, a test suitable for small sample sizes, and the two sets of data being compared were recorded from the same participant in different conditions.

References

1. Green, R. M. *et al.* Benefits, shortcomings, and costs of EEG monitoring. *Ann. Surg.* **201**, 785–92, DOI: [10.1097/0000658-198506000-00017](https://doi.org/10.1097/0000658-198506000-00017) (1985).
2. Henry, J. C. Electroencephalography: basic principles, clinical applications, and related fields. *Neurology* **67**, 2092–2092 (2006).

²Subscripts refer to the neuron’s index and superscripts refer to the layer containing the neuron, weight or bias

3. Britton, J. W. *et al.* *Electroencephalography (EEG): An Introductory Text and Atlas of Normal and Abnormal Findings in Adults, Children, and Infants* (American Epilepsy Society, 2016), 1 edn.
4. Jiang, X., Bian, G.-B. & Tian, Z. Removal of Artifacts from EEG Signals: A Review. *Sensors (Basel)* **19**, DOI: [10.3390/s19050987](https://doi.org/10.3390/s19050987) (2019).
5. Fatourehchi, M., Bashashati, A., Ward, R. K. & Birch, G. E. Emg and eeg artifacts in brain computer interface systems: A survey. *Clin. neurophysiology* **118**, 480–494 (2007).
6. McMenamin, B. W. *et al.* Validation of ica-based myogenic artifact correction for scalp and source-localized eeg. *NeuroImage* **49**, 2416–2432, DOI: [10.1016/j.neuroimage.2009.10.010](https://doi.org/10.1016/j.neuroimage.2009.10.010) (2010).
7. Fitzgibbon, S. P., Powers, D. M. W., Pope, K. J. & Clark, C. R. Removal of eeg noise and artifact using blind source separation. *J. clinical neurophysiology : official publication Am. Electroencephalogr. Soc.* **24**, 232–243, DOI: [10.1097/WNP.0b013e3180556926](https://doi.org/10.1097/WNP.0b013e3180556926) (2007).
8. Delorme, A., Sejnowski, T. & Makeig, S. Enhanced detection of artifacts in eeg data using higher-order statistics and independent component analysis. *NeuroImage* **34**, 1443–1449, DOI: [10.1016/j.neuroimage.2006.11.004](https://doi.org/10.1016/j.neuroimage.2006.11.004) (2007).
9. Nordin, A. D., Hairston, W. D. & Ferris, D. P. Human electrocortical dynamics while stepping over obstacles. *Sci Rep* **9**, 4693, DOI: [10.1038/s41598-019-41131-2](https://doi.org/10.1038/s41598-019-41131-2) (2019).
10. Jirayucharoensak, S., Israsena, P., Pan-ngum, S. & Hemrungronj, S. Online eeg artifact suppression for neurofeedback training systems. In *The 6th 2013 Biomedical Engineering International Conference*, 1–5 (IEEE, 2013).
11. Jirayucharoensak, S., Israsena, P., Pan-Ngum, S., Hemrungronj, S. & Maes, M. A game-based neurofeedback training system to enhance cognitive performance in healthy elderly subjects and in patients with amnesic mild cognitive impairment. *Clin. interventions aging* **14**, 347–360, DOI: [10.2147/CIA.S189047](https://doi.org/10.2147/CIA.S189047) (2019).
12. Ahmadi, A., Dehzangi, O. & Jafari, R. Brain-computer interface signal processing algorithms: A computational cost vs. accuracy analysis for wearable computers. In *2012 Ninth International Conference on Wearable and Implantable Body Sensor Networks*, 40–45, DOI: [10.1109/BSN.2012.19](https://doi.org/10.1109/BSN.2012.19) (2012).
13. Duvinage, M. *et al.* Biosignals and biorobotics conference (brc), 2012 issnip. *Piscataway, NJ: IEEE* (2012).
14. Kher, R. & Gandhi, R. Adaptive filtering based artifact removal from electroencephalogram (eeg) signals. In *2016 International Conference on Communication and Signal Processing (ICCSP)*, 0561–0564 (IEEE, 2016).
15. He, P., Wilson, G. & Russell, C. Removal of ocular artifacts from electro-encephalogram by adaptive filtering. *Med. biological engineering computing* **42**, 407–412 (2004).
16. Umlauf, C. W. A Simplified Basal Electrode for Routine EEG Use. *Science* **107**, 121, DOI: [10.1126/science.107.2770.121](https://doi.org/10.1126/science.107.2770.121) (1948).
17. McAdams, E. *Bioelectrodes* (American Cancer Society, 2006). <https://onlinelibrary.wiley.com/doi/pdf/10.1002/0471732877.emd013>.
18. Schwab, R. S. & Chock, Y. C. A circuit for checking both electrode continuity and resistance during EEG recording. *Electroencephalogr Clin Neurophysiol* **5**, 447–9, DOI: [10.1016/0013-4694\(53\)90089-3](https://doi.org/10.1016/0013-4694(53)90089-3) (1953).
19. Guger, C., Krausz, G., Allison, B. Z. & Edlinger, G. Comparison of dry and gel based electrodes for p300 brain-computer interfaces. *Front Neurosci* **6**, 60, DOI: [10.3389/fnins.2012.00060](https://doi.org/10.3389/fnins.2012.00060) (2012).
20. Xu, J., Mitra, S., Hoof, C. V., Yazicioglu, R. F. & Makinwa, K. A. A. Active Electrodes for Wearable EEG Acquisition: Review and Electronics Design Methodology. *IEEE Rev Biomed Eng* **10**, 187–198, DOI: [10.1109/RBME.2017.2656388](https://doi.org/10.1109/RBME.2017.2656388) (2017).
21. Krachunov, S. & Casson, A. 3d printed dry eeg electrodes. *Sensors* **16**, 1635, DOI: [10.3390/s16101635](https://doi.org/10.3390/s16101635) (2016).
22. Velcescu, A. *et al.* Flexible 3D-Printed EEG Electrodes. *Sensors (Basel)* **19**, DOI: [10.3390/s19071650](https://doi.org/10.3390/s19071650) (2019).
23. Nathan, V. & Jafari, R. Design Principles and Dynamic Front End Reconfiguration for Low Noise EEG Acquisition With Finger Based Dry Electrodes. *IEEE Trans Biomed Circuits Syst* **9**, 631–40, DOI: [10.1109/TBCAS.2015.2471080](https://doi.org/10.1109/TBCAS.2015.2471080) (2015).
24. Liao, L.-D., Wang, I.-J., Chen, S.-F., Chang, J.-Y. & Lin, C.-T. Design, fabrication and experimental validation of a novel dry-contact sensor for measuring electroencephalography signals without skin preparation. *Sensors (Basel)* **11**, 5819–34, DOI: [10.3390/s110605819](https://doi.org/10.3390/s110605819) (2011).
25. Clerc, M., Bougrain, L. & Lotte, F. Digital signal processing and machine learning. In *Brain-Computer Interfaces* (Springer, 2011).

26. Besio, G., Koka, K., Aakula, R. & Dai, W. Tri-polar concentric ring electrode development for laplacian electroencephalography. *IEEE Transactions on Biomed. Eng.* **53**, 926–933, DOI: [10.1109/tbme.2005.863887](https://doi.org/10.1109/tbme.2005.863887) (2006).
27. Makeyev, O., Ding, Q. & Besio, W. G. Improving the accuracy of laplacian estimation with novel multipolar concentric ring electrodes. *Measurement* **80**, 44–52, DOI: [10.1016/j.measurement.2015.11.017](https://doi.org/10.1016/j.measurement.2015.11.017) (2016).
28. Fitzgibbon, S. P. *et al.* Surface Laplacian of scalp electrical signals and independent component analysis resolve EMG contamination of electroencephalogram. *Int J Psychophysiol* **97**, 277–84, DOI: [10.1016/j.ijpsycho.2014.10.006](https://doi.org/10.1016/j.ijpsycho.2014.10.006) (2015).
29. Garcia-Casado, J., Ye-Lin, Y., Prats-Boluda, G. & Makeyev, O. Evaluation of bipolar, tripolar, and quadripolar laplacian estimates of electrocardiogram via concentric ring electrodes. *Sensors* **19**, 3780, DOI: [10.3390/s19173780](https://doi.org/10.3390/s19173780) (2019).
30. Aghaei-Lasboo, A. *et al.* Tripolar concentric eeg electrodes reduce noise. *Clin. Neurophysiol.* **131**, 193–198, DOI: [10.1016/j.clinph.2019.10.022](https://doi.org/10.1016/j.clinph.2019.10.022) (2020).
31. Rohaizad, N., Mayorga-Martinez, C. C., Novotny, F., Webster, R. D. & Pumera, M. 3d-printed ag/agcl pseudo-reference electrodes. *Electrochem. Commun.* **103**, 104–108, DOI: [10.1016/j.elecom.2019.05.010](https://doi.org/10.1016/j.elecom.2019.05.010) (2019).
32. Salvo, P. *et al.* A 3d printed dry electrode for ecg/eeg recording. *Sensors Actuators A: Phys.* **174**, 96–102, DOI: [10.1016/j.sna.2011.12.017](https://doi.org/10.1016/j.sna.2011.12.017) (2012).
33. Ntagios, M., Nassar, H., Pullanchiyodan, A., Navaraj, W. T. & Dahiya, R. Robotic hands with intrinsic tactile sensing via 3d printed soft pressure sensors. *Adv. Intell. Syst.* **2**, 1900080, DOI: [10.1002/aisy.201900080](https://doi.org/10.1002/aisy.201900080) (2019).
34. Chen, Y.-H. *et al.* Soft, comfortable polymer dry electrodes for high quality ecg and eeg recording. *Sensors* **14**, 23758–23780, DOI: [10.3390/s141223758](https://doi.org/10.3390/s141223758) (2014).
35. Di Flumeri, G. *et al.* The dry revolution: Evaluation of three different eeg dry electrode types in terms of signal spectral features, mental states classification and usability. *Sensors* **19**, 1365, DOI: [10.3390/s19061365](https://doi.org/10.3390/s19061365) (2019).
36. Lopez-Gordo, M., Sanchez-Morillo, D. & Valle, F. Dry eeg electrodes. *Sensors* **14**, 12847–12870, DOI: [10.3390/s140712847](https://doi.org/10.3390/s140712847) (2014).
37. Suarez-Perez, A. *et al.* Quantification of Signal-to-Noise Ratio in Cerebral Cortex Recordings Using Flexible MEAs With Co-localized Platinum Black, Carbon Nanotubes, and Gold Electrodes. *Frontiers in Neuroscience* **12**, DOI: [10.3389/fnins.2018.00862](https://doi.org/10.3389/fnins.2018.00862) (2018).
38. Daryanavard, S., Cowan, H., Porr, B. & Dahiya, R. Deep neuronal filter, DOI: [10.5281/zenodo.4131102](https://doi.org/10.5281/zenodo.4131102) (2020).
39. McFarland, D., McCane, L., David, S. & Wolpaw, J. Spatial filter selection for eeg-based communication. *Electroencephalogr. Clin. Neurophysiol.* **103**(3), 389–394 (1997).
40. Makeyev, O. Solving the general inter-ring distances optimization problem for concentric ring electrodes to improve laplacian estimation. *BioMedical Eng. OnLine* **17**, DOI: [10.1186/s12938-018-0549-6](https://doi.org/10.1186/s12938-018-0549-6) (2018).
41. Manjakkal, L., Dang, W., Yogeswaran, N. & Dahiya, R. Textile based potentiometric electrochemical ph sensor for wearable applications. *Biosensors* (2019).
42. Manjakkal, L., Dervin, S. & Dahiya, R. Flexible potentiometric ph sensors for wearable systems. *RSC Adv.* **10**, 8594–8617 (2020).
43. Mathewson, K. E., Harrison, T. J. L. & Kizuk, S. A. D. High and dry? Comparing active dry EEG electrodes to active and passive wet electrodes. *Psychophysiology* **54**, 74–82, DOI: [10.1111/psyp.12536](https://doi.org/10.1111/psyp.12536) (2017).
44. Gorecka, J. & Makiewicz, P. The dependence of electrode impedance on the number of performed eeg examinations. *Sensors* **19**, 2608, DOI: [10.3390/s19112608](https://doi.org/10.3390/s19112608) (2019).
45. Manjakkal, L., Sakthivel, D. & Dahiya, R. Flexible printed reference electrodes for electrochemical applications. *Adv. Mater. Technol.* **3** (2018).
46. Kalevo, L. *et al.* Effect of sweating on electrode-skin contact impedances and artifacts in eeg recordings with various screen-printed ag/agcl electrodes. *IEEE Access* **8**, 50934–50943, DOI: [10.1109/access.2020.2977172](https://doi.org/10.1109/access.2020.2977172) (2020).
47. Hayes, M. *Statistical Digital Signal Processing and Modeling* (John Wiley & Sons, 1996).
48. Islam, M. K., Rastegarnia, A. & Yang, Z. Methods for artifact detection and removal from scalp eeg: A review. *Neurophysiol. Clinique/Clinical Neurophysiol.* **46**, 287 – 305, DOI: <https://doi.org/10.1016/j.neucli.2016.07.002> (2016).
49. Daryanavard, S. & Porr, B. Closed-loop deep learning: Generating forward models with backpropagation. *Neural Comput.* **32**, 2122–2144 (2020).

50. Mateo, J., Torres, A. M. & García, M. A. Eye interference reduction in electroencephalogram recordings using a radial basis function. *IET Signal Process.* **7**, 565–576 (2013).
51. Jafarifarmand, A. & Badamchizadeh, M. A. Artifacts removal in eeg signal using a new neural network enhanced adaptive filter. *Neurocomputing* **103**, 222 – 231, DOI: <https://doi.org/10.1016/j.neucom.2012.09.024> (2013).
52. Hu, J. *et al.* Removal of eog and emg artifacts from eeg using combination of functional link neural network and adaptive neural fuzzy inference system. *Neurocomputing* **151**, 278 – 287, DOI: <https://doi.org/10.1016/j.neucom.2014.09.040> (2015).
53. Yang, B., Duan, K., Fan, C., Hu, C. & Wang, J. Automatic ocular artifacts removal in eeg using deep learning. *Biomed. Signal Process. Control.* **43**, 148 – 158, DOI: <https://doi.org/10.1016/j.bspc.2018.02.021> (2018).
54. Nguyen, H.-A. T. *et al.* Eog artifact removal using a wavelet neural network. *Neurocomputing* **97**, 374–389 (2012).

Author contributions statement

B.P. and R.D conceived the experiment(s), H.C. conducted the experiment(s), S.D. and B.P. analysed the results. All authors reviewed the manuscript.

Additional information

Competing interests B.P. is CEO of Glasgow Neuro LTD which manufactures the Attys DAQ board.